Open-ocean convection becoming less intense in the Greenland and Iceland Seas

G.W.K. Moore

Department of Physics

University of Toronto, Canada

K. Våge

Geophysical Institute, University of Bergen and Bjerknes Centre for Climate Research, Bergen, Norway

R.S. Pickart

Department of Physical Oceanography

Woods Hole Oceanographic Institution, USA

I.A. Renfrew

Centre for Ocean and Atmospheric Sciences,

School of Environmental Sciences

University of East Anglia, UK

Manuscript in press Nature Climate Change

May 18, 2015

The air-sea transfer of heat and freshwater plays a critical role in the global climate system[1]. This is particularly true for the Greenland and Iceland Seas, where these fluxes drive ocean convection that contributes to Denmark Strait Overflow Water, the densest component of the lower limb of the Atlantic Meridional Overturning Circulation (AMOC)[2]. Here we show that the wintertime retreat of sea ice in the region, combined with different rates of warming for the atmosphere and sea surface of the Greenland and Iceland Seas, has resulted in statistically significant reductions of approximately 20% in the magnitude of the winter air-sea heat fluxes since 1979. We also show that modes of climate variability other than the North Atlantic Oscillation (NAO)[3-7] are required to fully characterize the regional air-sea interaction. Mixed-layer model simulations imply that further decreases in atmospheric forcing will exceed a threshold for the Greenland Sea whereby convection will become depth limited, reducing the ventilation of mid-depth waters in the Nordic Seas. In the Iceland Sea, further reductions have the potential to decrease the supply of the densest overflow waters to the AMOC[8].

Sea ice in the Iceland and Greenland Seas has undergone dramatic fluctuations since 1900[9] (Fig. 1). In particular, the early 20th Century warming period from the 1920s-1940s[10] was characterized by reduced ice extent, while there was an expansion of sea ice during the mid-century cooling period from the 1960s-1970s[11]. The reduction in sea ice concentration that has occurred over the past 30 years is unprecedented in this 111 year long record and has resulted in the lowest sea ice extent in the region since the 1200s[12].

41 The Iceland and Greenland Seas contain gyres (Fig. 1) where oceanic convection
42 occurs[8,13,14], a process that is crucial for dense water formation and thus the AMOC[5].
43 Open-ocean convection requires a suitably preconditioned environment, typically a
44 cyclonic gyre which domes the isopycnals resulting in a weakly stratified mid-depth
45 water column. This makes it easier for convective overturning to extend to greater depths
46 once the surface waters lose buoyancy through the transfer of heat and moisture to the
47 atmosphere[13]. The buoyancy loss tends to be largest at the ice edge, where cold and dry
48 Arctic air first comes into contact with the relatively warm surface waters[15]. The recent
49 retreat of wintertime sea ice (Figure 1) has increased the distance of these two oceanic
50 gyres from the ice edge and hence the region of largest heat loss. Here we address how
51 this change is affecting ocean convection.
52 We focus on the changes in winter mean conditions for the period 1958-2014,
53 using a merged dataset, described in the Supplementary Material, consisting of the 40-
54 year (ERA-40) and the Interim (ERA-I) Reanalyses, both from the European Centre for
55 Medium-Range Weather Forecasts[16,17]. As can be seen from Figure 1, this time period
56 covers both the mid-century cooling, in which there was an expansion of sea ice in the
57 vicinity of both convection sites, as well as the more recent period with unprecedented
58 retreat of ice across the entire region.
59 Figure 2 shows the winter mean sea ice concentration within the two gyres, as
60 well as the turbulent heat flux Q_{thf}^{ocean} within the open water portion of the gyres (error
61 estimates described in the Supplementary Material). Consistent with Figure 1, both gyres
62 had their highest sea ice concentrations in the late 1960s. Since that time, sea ice cover in

63 the Iceland Sea gyre has vanished, while in the Greenland Sea it persisted until the mid
64 1990s after which it also disappeared. The time series of Q_{thf}^{ocean} shows that both gyres are
65 subject to considerable inter-annual variability in atmospheric forcing as well as long-
66 term tendencies towards reduced fluxes. This low-frequency variability has been assessed
67 using Singular Spectrum Analysis (SSA), a non-parametric spectral analysis technique
68 that uses data-adaptive basis functions to partition a time series into components that
69 maximizes the described variability in the original time series[18]. For the Iceland Sea site,
70 the low-frequency SSA reconstruction indicates that there has been a steady reduction in
71 Q_{thf}^{ocean} since the time of the region's sea ice maximum in the late 1960s. For the
72 Greenland Sea site, the reconstruction indicates that the period of interest is characterized
73 by small-amplitude multi-decadal variability with a trend towards lower values that
74 began in the mid-1990s, and which coincides with the onset of ice-free conditions in the
75 gyre. As shown in Figure 1, there is nevertheless still sea ice present to the northwest of
76 both gyres.

77 As discussed in the Supplementary Material, the correlation of Q_{thf}^{ocean} over both
78 gyres with the winter mean index of the NAO, the leading mode of climate variability in
79 the North Atlantic[4], is not statistically significant. This suggests, in agreement with
80 previous studies[7,19], that modes of variability other than the NAO are needed to fully
81 describe the climate in the region.

82 Piecewise continuous linear least-squares fits to Q_{thf}^{ocean} at both sites with
83 breakpoints consistent with the SSA low-frequency behavior (1970 for the Iceland Sea

84 and 1992 for the Greenland Sea) are also shown in Figure 2. At both sites, the trends after
85 the breakpoints are statistically significant at the 95th percentile confidence interval. As
86 described in the Supplementary Material, all significance tests presented here take into
87 account the 'red noise' characteristic of geophysical time series. Indeed, since 1979 there
88 has been a reduction in the magnitude of Q_{thf}^{ocean} over both gyres of approximately 20%.
89 Similar results hold if one includes the net radiative flux to obtain the total heat flux over
90 the open ocean (Supplementary Figure 1).

91 The turbulent heat flux Q_{thf}^{ocean} is the sum of the sensible and latent heat fluxes.
92 These components tend to be spatially similar, and, in this region, the sensible heat flux
93 usually dominates[6]. The sensible heat flux is parameterized as being proportional to the
94 product of the 10m wind speed and the air-sea temperature difference[20]. The time series
95 of the latter, as well as their low-frequency SSA reconstructions over the two convection
96 sites, are also shown in Figure 2 and indicate a tendency for a reduced air-sea temperature
97 difference in recent years over both sites. This is due to the atmosphere warming at a
98 faster rate than the ocean thus leading to a reduction in Q_{thf}^{ocean}. Figure 2 indicates that there
99 has been a recent reduction in the 10m wind speed over the Iceland Sea that is also
100 contributing to the Q_{thf}^{ocean} trend. In contrast, the 10m wind speeds over the Greenland Sea
101 indicate the presence of multi-decadal variability but no trend.

102 Unfortunately there are no suitably long oceanographic time series with which to
103 document the oceanic response to this reduction in the atmospheric forcing over the
104 Greenland and Iceland Seas. As such, we employ a one-dimensional mixed-layer model,

105 known as the PWP[21] model, to simulate the wintertime evolution of the mixed-layer in
106 the two gyres under various forcing conditions. Please see the Supplementary Material
107 for details. Initial conditions for the PWP model are specified using a collection of
108 October and November hydrographic profiles from within the gyres, obtained from the
109 NISE[22] data base and the Argo profiling float programme over the period 1980 to present
110 (Fig. 3).

111 The autumn hydrographic profiles reveal that, near the surface, there is substantial
112 variability which rapidly decreases with depth (Fig. 3a,b). The variability is more
113 pronounced in the Greenland Sea, but, in the mean, the density in the upper part of the
114 water column is greater in the Greenland Sea than in the Iceland Sea. Below ~700 m the
115 situation is reversed and the Iceland Sea is more dense (Fig. 3c). Local ventilation in the
116 Iceland Sea does not reach these depths, so the waters there were formed upstream in
117 either the Greenland Sea or the Arctic Ocean and subsequently spread into the Iceland
118 Sea[14]. More recently formed intermediate waters in the Greenland Sea (after the cessation
119 of bottom water production there[23]) are less dense. As a result of these factors, the upper
120 ~1500 m of the Greenland Sea is less stratified than the Iceland Sea. This, together with
121 the substantially higher heat fluxes of the Greenland Sea (Fig. 2), are the major
122 contributors to deeper convection within the Greenland Sea gyre as compared to the
123 Iceland Sea gyre[13].

124 To gauge the effectiveness of the PWP model, we used the Argo data to identify
125 a weak (2012) and a strong (2008) convective year in the Nordic Seas. Using the
126 November hydrographic profiles for individual Argo floats as initial conditions, we

127 compared the evolution of the mixed-layer depth (MLD) in the model (forced by 6-
128 hourly atmospheric fluxes from the ERA-I reanalysis product) to the float observations in
129 each gyre (Supp. Fig 2). The results are qualitatively comparable, given the stochastic
130 nature of convection, and indicate that the model is able to capture the seasonal evolution
131 of the mixed-layer in both regions as well as its inter-annual variability.

132 Using a range of initial conditions, we investigated the sensitivity of convection in
133 the Greenland and Iceland Seas to the atmospheric forcing (Figure 4). In particular, we
134 calculated the maximum late-winter MLD attained in each gyre using the mean autumn
135 hydrographic profiles as initial conditions (Fig. 3c) and a prescribed constant atmospheric
136 forcing over the entire winter period from 1 November to 30 April. We note that these
137 constant levels of forcing are idealised and do not take into account synoptic-scale high
138 heat flux events[15], which can impact the wintertime evolution of the mixed-layer[24]. Tests
139 with more realistic six-hourly forcing generally produced slightly deeper mixed-layers,
140 but were comparable to those from the corresponding constant-forcing simulations.

141 Our model results confirm that the likelihood of deep convection is much higher
142 in the Greenland Sea. For example, the maximum model MLD, for the largest observed
143 mean winter forcing, is 1000 m in the Greenland Sea versus only 500 m in the Iceland
144 Sea. The model results also reveal an unanticipated difference in the behaviour of oceanic
145 convection between the gyres. In the Iceland Sea there is a nearly linear relationship
146 between the maximum MLD and the winter-mean heat flux, throughout the range of
147 forcing (~5 m change in MLD for every 1 W m^{-2}). In contrast, the Greenland Sea is
148 characterized by two distinct convective regimes. For atmospheric forcing less than about

149 150 W m^{-2}, the MLD only increases moderately with heat flux (~3 m change in MLD for
150 every 1 W m^{-2}). However, for heat fluxes exceeding this value, the MLD is significantly
151 more sensitive to the forcing (~10 m change in MLD for every 1 W m^{-2}). This threshold
152 behaviour is due to the background stratification of the Greenland Sea (Fig. 4b).
153 Consequently, if the winter is sufficiently severe to erode the stratification of the upper
154 layer, the weakly stratified waters below the pycnocline present little resistance to deeper
155 convection.

156 Over the past 30 years the range of mean wintertime atmospheric forcing falls
157 within both of these convective regimes for the Greenland Sea, and shallow as well as
158 deep mixed-layers have been observed and simulated (e.g. Supp Fig 2). However, taking
159 into consideration the negative trend of atmospheric forcing documented above (Fig. 2),
160 which is also illustrated by the reduced mean of the 1997-2014 period relative to the
161 1979-1996 period (see Fig. 4), the Greenland Sea may be undergoing a transition from a
162 state of intermediate depth convection to one in which only shallow convection occurs. If
163 this trend continues, the production of intermediate waters in the Greenland Sea, and
164 hence the ventilation of a substantial volume of the Nordic Seas, may be at stake. In the
165 Iceland Sea, the nearly linear convective regime implies a more gradual reduction in
166 convective depth. However, if the decrease in wintertime atmospheric forcing in this
167 region (already 20% smaller than 30 years ago) continues, it will weaken the overturning
168 loop that feeds the North Icelandic Jet[8], thus reducing the supply of the densest water to
169 the AMOC. A measurement system now in place in the Denmark Strait should be able to
170 measure any such changes in properties of the overflow water.

171 Observations, proxies and model simulations suggest that a recent weakening of
172 the AMOC has occurred[25,26]. Furthermore, models predict that such a slow down will
173 continue as a result of increasing greenhouse gas concentrations[26,27]. Such a weakening
174 of the AMOC would have dramatic impacts on the climate of the North Atlantic and
175 western Europe[28]. Although there is considerable debate regarding the dynamics of the
176 AMOC[29], one proposed mechanism for its current and predicted decline is a freshening
177 of the surface waters – for instance due to enhanced meltwater emanating from the
178 Greenland Ice Sheet – that reduces their density making it more difficult for oceanic
179 convection to occur[26,27] However, much of the freshwater discharge from the Greenland
180 Ice Sheet is apt to be exported equatorward via the boundary current system surrounding
181 Greenland[30] with limited direct spreading into the interior basins adjacent to the ice sheet
182 where oceanic convection occurs. Further work is thus necessary to determine how and
183 where – and on what timescales - this freshwater pervades the northwest Atlantic. Our
184 results suggest that other possible mechanisms for such a slowdown in the AMOC may
185 be at work; such as a reduction in the magnitude of the surface heat fluxes that trigger
186 the overturning.

187 ***Please direct all correspondence and request for materials to Professor G.W.K. Moore***
188 ***(gwk.moore@utoronto.ca).***

189 **Acknowledgements**

190 The authors would like to thank the European Centre for Medium-Range Weather
191 Forecasts for access to the ERA-40 and ERA-I reanalyses. GWKM was supported by the
192 Natural Sciences and Engineering Research Council of Canada. KV has received funding

from NACLIM, a project of the European Union 7th Framework Programme (FP7 2007-2013) under grant agreement no. 308299, and from the Research Council of Norway under grant agreement no. 231647. RSP was supported by the US National Science Foundation. IAR has received funding from the Natural Environmental Research Council for the ACCACIA project (NE/I028297/1).

Author contributions

GWKM, KV, RSP and IAR jointly conceived the study. GWKM analysed the atmospheric reanalyses and sea ice data sets. KV carried out the ocean mixed-layer modelling. All authors jointly interpreted the results and wrote the manuscript.

Additional information

Supplementary figures are available for this article.

Competing financial interests

The authors declare no competing financial interests.

References

1 Curry, J. A. *et al*. Seaflux. *Bulletin of the American Meteorological Society* **85**, 409-+, doi:10.1175/bams-85-3-409 (2004).

2 Mauritzen, C. Production of dense overflow waters feeding the North Atlantic across the Greenland-Scotland Ridge .1. Evidence for a revised circulation scheme. *Deep-Sea Research Part I-Oceanographic Research Papers* **43**, 769-806, doi:10.1016/0967-0637(96)00037-4 (1996).

3 Dickson, B. From the Labrador Sea to global change. *Nature* **386**, 649-650, doi:10.1038/386649a0 (1997).

4 Hurrell, J. W. Decadal trends in the North-Atlantic Oscillation - regional temperatures and precipitation. *Science* **269**, 676-679, doi:10.1126/science.269.5224.676 (1995).

5 Jahnke-Bornemann, A. & Bruemmer, B. The Iceland-Lofotes pressure difference: different states of the North Atlantic low-pressure zone. *Tellus Series a-Dynamic Meteorology and Oceanography* **61**, 466-475, doi:10.1111/j.1600-0870.2009.00401.x (2009).

6 Moore, G. W. K., Renfrew, I. A. & Pickart, R. S. Spatial distribution of air-sea heat fluxes over the sub-polar North Atlantic Ocean. *Geophysical Research Letters* **39**, doi:10.1029/2012gl053097 (2012).

7 Moore, G. W. K., Renfrew, I. A. & Pickart, R. S. Multidecadal Mobility of the North Atlantic Oscillation. *Journal of Climate* **26**, 2453-2466, doi:10.1175/jcli-d-12-00023.1 (2013).

8 Våge, K. *et al*. Significant role of the North Icelandic Jet in the formation of Denmark Strait overflow water. *Nature Geoscience* **4**, 723-727, doi:10.1038/ngeo1234 (2011).

9 Titchner, H. A. & Rayner, N. A. The Met Office Hadley Centre sea ice and sea surface temperature data set, version 2: 1. Sea ice concentrations. *Journal of Geophysical Research-Atmospheres* **119**, 2864-2889, doi:10.1002/2013jd020316 (2014).

10 Bengtsson, L., Semenov, V. A. & Johannessen, O. M. The early twentieth-century warming in the Arctic - A possible mechanism. *Journal of Climate* **17**, 4045-4057, doi:10.1175/1520-0442(2004)017<4045:tetwit>2.0.co;2 (2004).

11 Shindell, D. & Faluvegi, G. Climate response to regional radiative forcing during the twentieth century. *Nature Geoscience* **2**, 294-300, doi:10.1038/ngeo473 (2009).

12 Fauria, M. M. *et al*. Unprecedented low twentieth century winter sea ice extent in the Western Nordic Seas since AD 1200. *Climate Dynamics* **34**, 781-795, doi:10.1007/s00382-009-0610-z (2010).

13 Marshall, J. & Schott, F. Open-ocean convection: Observations, theory, and models. *Reviews of Geophysics* **37**, 1-64, doi:10.1029/98rg02739 (1999).

14 Swift, J. H., Aagaard, K. & Malmberg, S. A. Contribution of the Denmark Strait overflow to the deep North-Atlantic. *Deep-Sea Research Part a-Oceanographic Research Papers* **27**, 29-42, doi:10.1016/0198-0149(80)90070-9 (1980).

15 Renfrew, I. A. & Moore, G. W. K. An extreme cold-air outbreak over the Labrador Sea: Roll vortices and air-sea interaction. *Monthly Weather Review* **127**, 2379-2394, doi:10.1175/1520-0493(1999)127<2379:aecaoo>2.0.co;2 (1999).

16 Uppala, S. M. *et al*. The ERA-40 re-analysis. *Quarterly Journal of the Royal Meteorological Society* **131**, 2961-3012, doi:10.1256/qj.04.176 (2005).

17 Dee, D. P. *et al*. The ERA-Interim reanalysis: configuration and performance of the data assimilation system. *Quarterly Journal of the Royal Meteorological Society* **137**, 553-597, doi:10.1002/qj.828 (2011).

18 Ghil, M. *et al*. Advanced spectral methods for climatic time series. *Reviews of Geophysics* **40**, doi:10.1029/2000rg000092 (2002).

19 Kelly, P. M., Goodess, C. M. & Cherry, B. S. G. The interpretation of the Icelandic sea ice record. *Journal of Geophysical Research-Oceans* **92**, 10835-10843, doi:10.1029/JC092iC10p10835 (1987).

20 Renfrew, I. A., Moore, G. W. K., Guest, P. S. & Bumke, K. A comparison of surface layer and surface turbulent flux observations over the Labrador Sea with ECMWF analyses and NCEP reanalyses. *Journal of Physical Oceanography* **32**, 383-400, doi:10.1175/1520-0485(2002)032<0383:acosla>2.0.co;2 (2002).

21 Price, J. F., Weller, R. A. & Pinkel, R. Diurnal cycling: Observations and models of the upper ocean response to diurnal heating, cooling, and wind mixing. *Journal of Geophysical Research-Atmospheres* **91**, 8411–8427 (1986).

22 Nilsen, J. E. Ø., Hatun, H., Mork, K. A. & Valdimarsson, H. The NISE data set., (Faroese Fisheries Laboratory, Torshavn, Faroe Islands, 2008).

23 Ronski, S. & Budeus, G. Time series of winter convection in the Greenland Sea. *Journal of Geophysical Research-Oceans* **110**, doi:10.1029/2004jc002318 (2005).

24 Våge, K., Pickart, R. S., Moore, G. W. K. & Ribergaard, M. H. Winter mixed-layer development in the central Irminger Sea: The effect of strong, intermittent wind events. *Journal of Physical Oceanography* **38**, 541–565 (2008).

25 Smeed, D. A. *et al*. Observed decline of the Atlantic meridional overturning circulation 2004-2012. *Ocean Science* **10**, 29-38, doi:10.5194/os-10-29-2014 (2014).

26 Rahmstorf, S. *et al*. Exceptional twentieth-century slowdown in Atlantic Ocean overturning circulation. *Nature Clim. Change* **advance online publication**, doi:10.1038/nclimate2554 (2015).

27 Wood, R. A., Keen, A. B., Mitchell, J. F. B. & Gregory, J. M. Changing spatial structure of the thermohaline circulation in response to atmospheric CO2 forcing in a climate model. *Nature* **399**, 572-575 (1999).

28 Bryden, H. L., Longworth, H. R. & Cunningham, S. A. Slowing of the Atlantic meridional overturning circulation at 25 degrees N. *Nature* **438**, 655-657, doi:10.1038/nature04385 (2005).

29 Kuhlbrodt, T. *et al*. On the driving processes of the Atlantic meridional overturning circulation. *Reviews of Geophysics* **45**, doi:10.1029/2004rg000166 (2007).

30 Sutherland, D. A. & Pickart, R. S. The East Greenland Coastal Current: Structure, variability, and forcing. *Progress in Oceanography* **78**, 58-77, doi:http://dx.doi.org/10.1016/j.pocean.2007.09.006 (2008).

296 **Figure Captions**

297 **Figure 1 Winter sea ice extent for the Nordic Seas.** Panels (a) to (d) show four decadal
298 mean maps of sea ice concentration (%) for (a) 1900-1909; (b) 1930-1939; (c)
299 1960-1969 and (d) 2000-2009. Panel (e) shows the time series of winter mean sea
300 ice area ($10^4 km^2$) for the region indicated by the white boxes in (a)-(d) for the
301 period 1900-2010. The decadal means for the periods shown in (a)-(d) are in blue
302 with the other decadal means in red. In (a) - (d), the gyres in the Iceland and
303 Greenland Seas where oceanic convection occurs are indicated by the thick black
304 and magenta curves respectively.

305 **Figure 2 Time series of the winter mean conditions over the Iceland and Greenland**
306 **Sea gyres.** Panels (a) and (b) show the sea ice concentration (%);(c) and (d) show
307 the open ocean turbulent heat flux with the shading representative of the
308 uncertainty associated with the sea ice concentration; (e) and (f) show the air-sea
309 temperature difference (ºC); (g) and (h) show the 10m wind speed ($m\ s^{-1}$). The red
310 curves are the SSA reconstructions of the low frequency variability in the time
311 series, while the blue lines in are continuous piecewise linear least squares fits.
312 The trend lines that are solid are statistically significant at the 95% confidence
313 level.

314 **Figure 3 Potential density profiles for October and November used as initial**
315 **conditions for the PWP model.** Panels are for a) the Greenland Sea and b) the
316 Iceland Sea. The traces are individual profiles (gray), means of the 20 percent

most- and least-stratified profiles (orange and cyan), and overall means (red and blue). Panel c) compares the mean profile from each gyre.

Figure 4 Relationship between end-of-winter simulated mixed-layer depths from the PWP model and the atmospheric forcing as represented by the winter mean open ocean turbulent heat flux. Panels a) and b) represent the Greenland and Iceland Sea gyres, respectively. The thick red and blue curves show the final mixed-layer depths resulting from the mean initial conditions, and the thin orange and cyan curves show the final mixed-layer depths resulting from the strongly and weakly stratified initial conditions. The shaded areas indicate the ranges of winter mean atmospheric forcing for the period 1979-2014, while the dashed lines represent the mean atmospheric forcing for the periods 1979-1996 and 1996-2014.

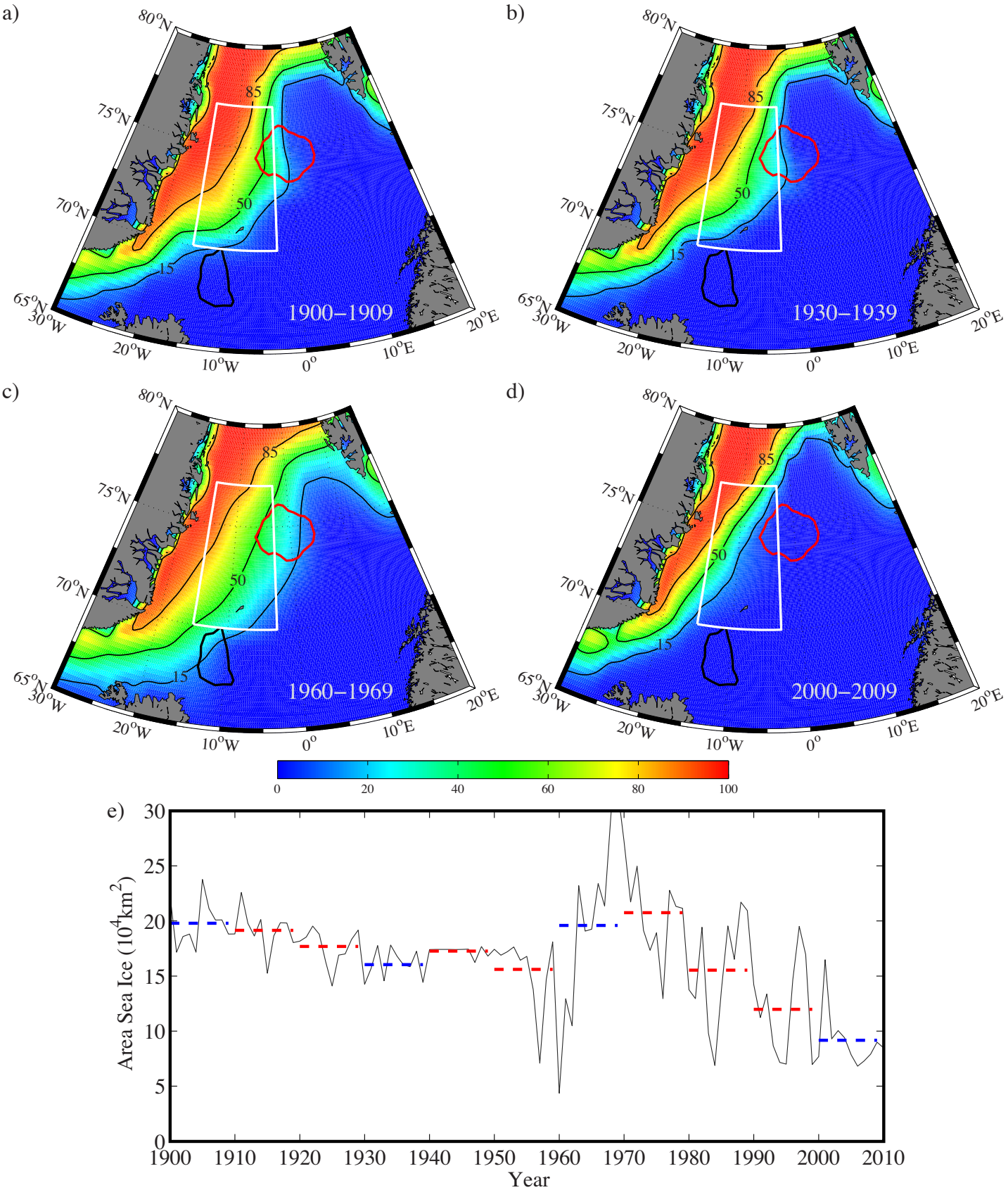

Figure 1 Winter sea ice extent for the Nordic Seas. Panels (a) to (d) show four decadal mean maps of sea ice concentration (%) for (a) 1900-1909; (b) 1930-1939; (c) 1960-1969 and (d) 2000-2009. Panel (e) shows the time series of winter mean sea ice area (10^4km^2) for the region indicated by the white boxes in (a)-(d) during 1900-2010. The decadal means for the periods shown in (a)-(d) are in blue with the other decadal means in red. In (a) - (d), the gyres in the Iceland and Greenland Seas where oceanic convection occurs are indicated by the thick black and magenta curves respectively.

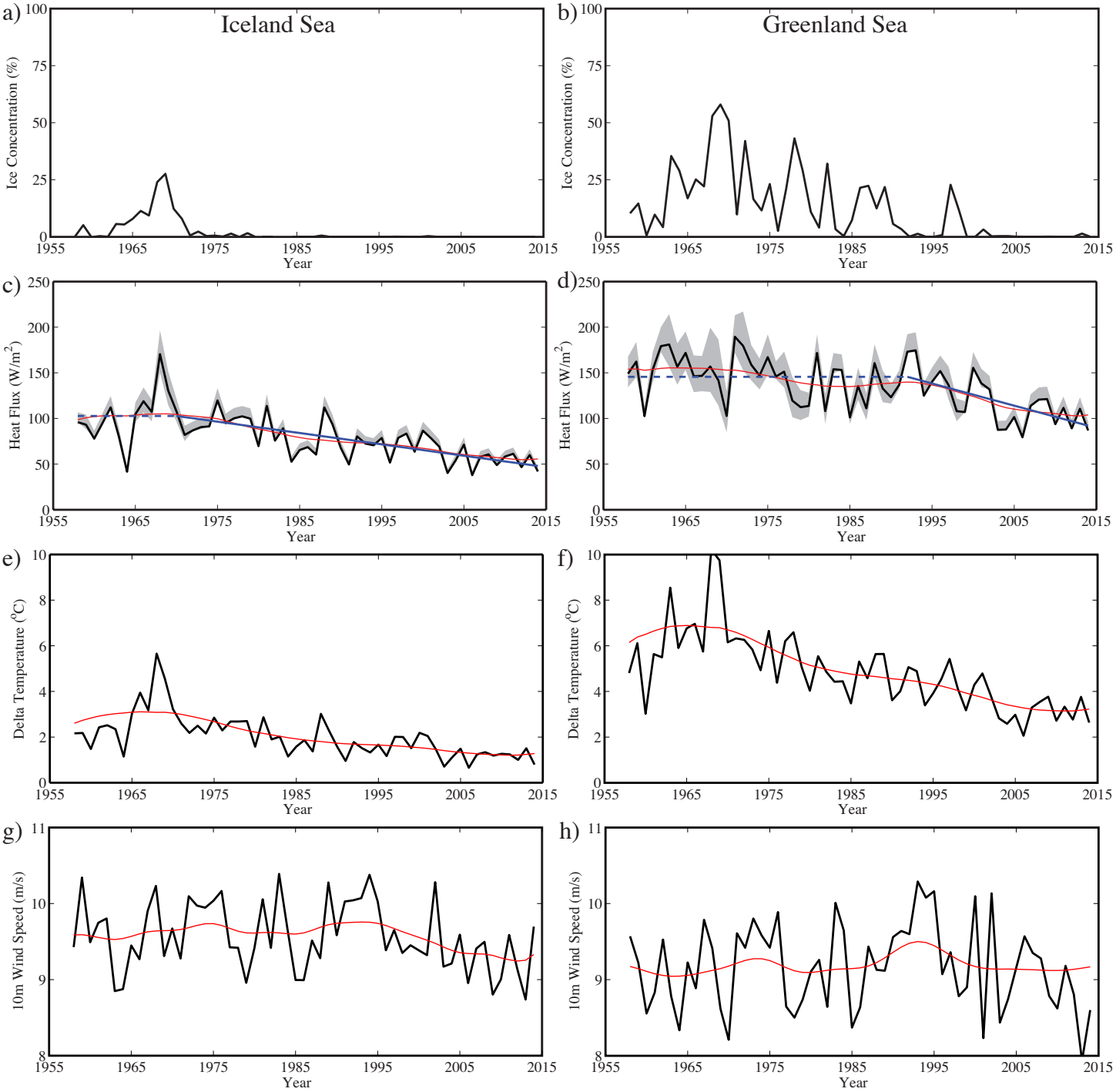

Figure 2 Time series of the winter mean conditions over the Iceland and Greenland Sea gyres. Panels (a) and (b) show the sea ice concentration (%);(c) and (d) show the open ocean turbulent heat flux with the shading representative of the uncertainty associated with the sea ice concentration (Wm^{-2}); (e) and (f) show the air-sea temperature difference (^oC); (g) and (h) show the 10m wind speed ($m\ s^{-1}$). The red curves are the SSA reconstructions of the low frequency variability in the time series, while the blue lines in are continuous piecewise linear least squares fits. The trend lines that are solid are statistically significant at the 95% confidence level.

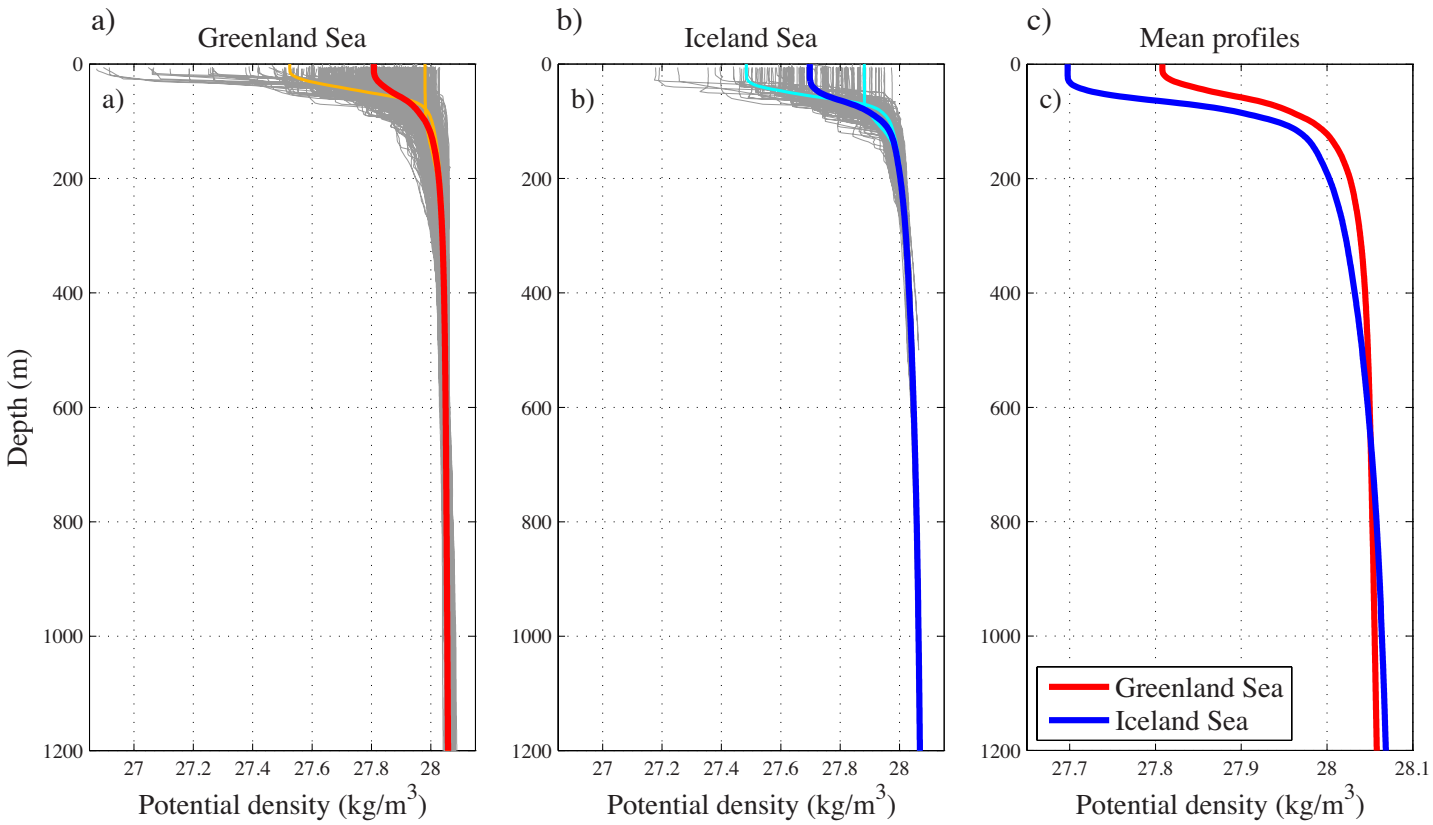

Figure 3 Potential density profiles for October and November used as initial conditions for the PWP model. Panels are for a) the Greenland Sea and b) the Iceland Sea. The traces are individual profiles (gray), means of the 20 percent most- and least-stratified profiles (orange and cyan), and overall means (red and blue). Panel c) compares the mean profile from each gyre.

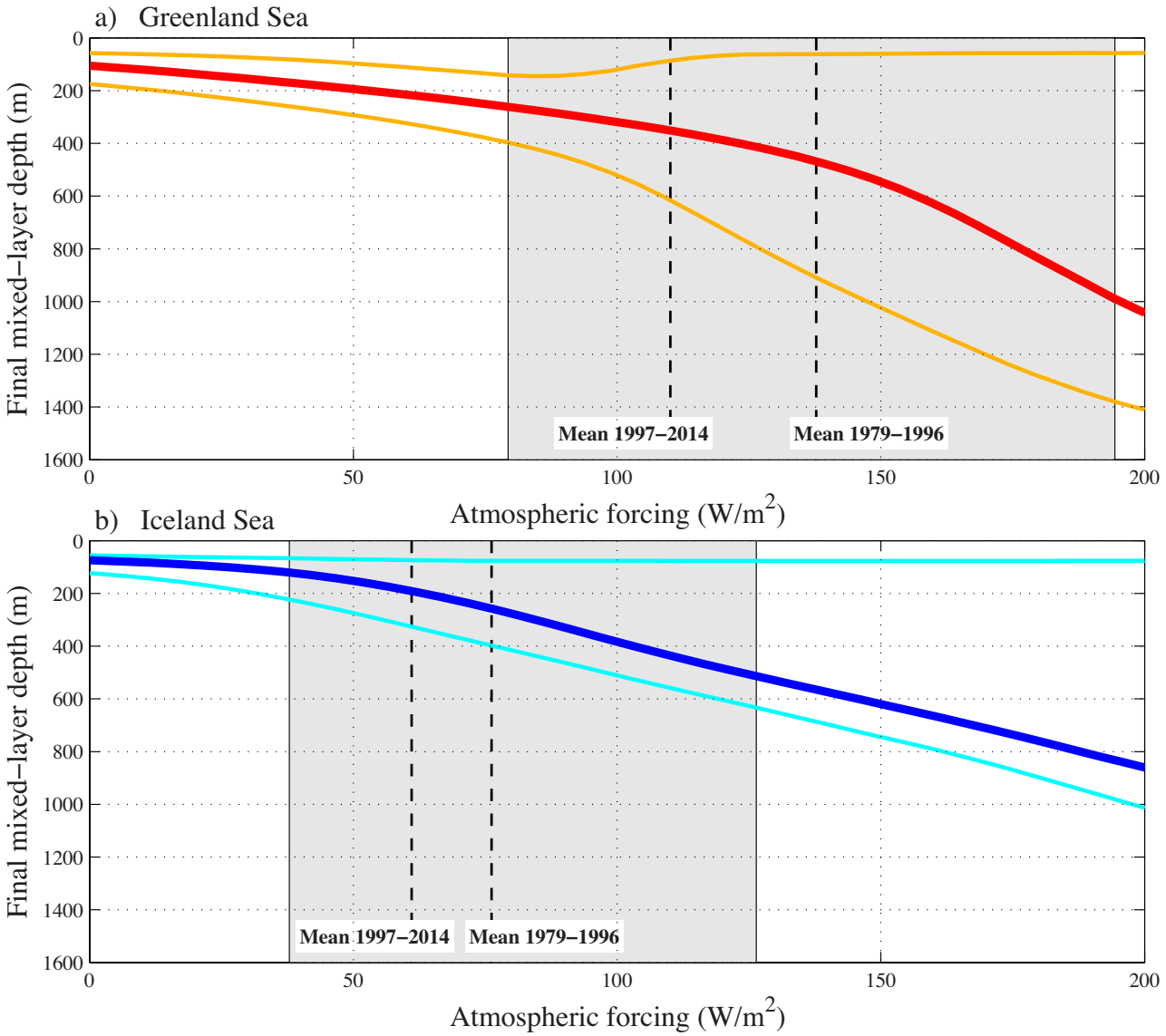

Figure 4 Relationship between end-of-winter simulated mixed-layer depths from the PWP model and the atmospheric forcing as represented by the winter mean open ocean turbulent heat flux. Panels a) and b) represent the Greenland and Iceland Sea gyres, respectively. The thick red and blue curves show the final mixed-layer depths resulting from the mean initial conditions, and the thin orange and cyan curves show the final mixed-layer depths resulting from the strongly and weakly stratified initial conditions. The shaded areas indicate the ranges of winter mean atmospheric forcing for the period 1979-2014, while the dashed lines represent the mean atmospheric forcing for the periods 1979-1996 and 1996-2014.